Seeding Convective Clouds with Hygroscopic Flares: Numerical Simulations Using a Cloud Model with Detailed Microphysics

YAN YIN, ZEV LEVIN, TAMIR REISIN, AND SHALVA TZIVION

Department of Geophysics and Planetary Sciences, Raymond and Beverly Sackler Faculty of Exact Sciences, Tel Aviv University, Ramat Aviv, Israel

(Manuscript received 4 June 1999, in final form 21 November 1999)

ABSTRACT

Numerical experiments were conducted to evaluate the role of hygroscopic flare seeding on enhancement of precipitation in convective clouds. The spectra of seeding particles were based on measurements of the particles produced by hygroscopic flares used in field experiments in South Africa. The seeding effects were investigated by comparing the development of precipitation particles and rain production between the seeded and unseeded cases for clouds with different cloud condensation nuclei (CCN) concentrations and spectra.

The South African hypothesis that the introduction of larger and more efficient artificial CCN below cloud base at the early stage of cloud development would influence the initial condensation process in the cloud, resulting in a broader droplet spectrum and in acceleration of the precipitation growth by coalescence, was tested. The results show that the largest seeding particles broaden the cloud droplet distribution near cloud base, leading to an earlier formation of raindrops, graupel particles, and, therefore, stronger radar echoes at a lower altitude. The results also show that the large artificial CCN prevent some of the natural CCN from becoming activated. It was found that seeding with the full particle spectrum from the flares could increase rainfall amount in continental clouds having CCN concentrations of more than about 500 cm^{-3} (active at 1% supersaturation). Seeding more maritime clouds resulted in reducing the integrated rain amount, although in some cases rain formation was accelerated. The physical mechanisms responsible for these results were explored by investigating the relative importance of different segments of the size spectrum of the seeding particles to precipitation development. It was found that, out of the full spectrum, the most effective particles were those with radii larger than 1 μm, especially those larger than 10 μm; the particles smaller than 1 μm always had a negative effect on the rain development.

The sensitivity of seeding effects to seeding time, seeding height, and seeding amounts also was tested. The biggest precipitation enhancement was obtained when seeding was conducted a few minutes after cloud initiation and above cloud base. The radar reflectivity at that time period was lower than 0 dBZ. Rain enhancement also increased with the increase in the concentration of the large seeding particles in the spectrum (at least for the amounts tested here).

1. Introduction

Hygroscopic seeding as a method to enhance rainfall by promoting the coalescence process is not new (e.g., Bowen 1952). Because in cold clouds precipitation development by the growth of ice particles is thought to be more efficient than growth by coagulation of drops, hygroscopic seeding mostly has been used and discussed in relation to warm clouds (e.g., Biswas and Dennis 1971; Tzivion et al. 1994; Czys and Bruintjes, 1994). In addition, the inconvenience encountered in practical operations [usually a much larger amount of seeding material needs to be dispersed in hygroscopic seeding; e.g., Reisin et al. (1996a)] also made this method less attractive than ice nuclei seeding. Recently, however, hygroscopic seeding with flares conducted in summertime convective clouds in South Africa and the promising results obtained in the field operations (Mather and Terblanche 1992; Mather et al. 1997; Bigg 1997) aroused renewed interest, because this kind of seeding approach may serve as an alternative to glaciogenic seeding in many parts of the world.

The experiments conducted in South Africa differ from earlier hygroscopic cloud seeding in that relatively modest amounts of more finely dispersed particles (mainly potassium chloride with 0.5-μm mean diameter) were introduced into the updrafts below cloud base from flares carried on an aircraft. The hypothesis for this new approach is that the larger and more efficient artificial CCN provided by flares would influence the initial condensation process in the cloud, resulting in a broader droplet spectrum at the early stage of the cloud's

Corresponding author address: Prof. Zev Levin, Dept. of Geophysics and Planetary Sciences, Tel Aviv University, Ramat Aviv 69978, Israel.
E-mail: zev@hail.tau.ac.il

© 2000 American Meteorological Society

Unauthenticated | Downloaded 07/13/24 07:39 PM UTC

lifetime and in acceleration of the precipitation growth by the coalescence process (Mather et al. 1997; Cooper et al. 1997). There are many operational advantages to this method. The amount of hygroscopic material required is not large, the particles are readily produced by flares, the target area for seeding is a relatively easily identified region at cloud base where the updrafts occur and where the initial droplet spectrum is formed. The results from the experiments indicated that the radar-measured rain from seeded storms was more intensive and lasted longer than that from the unseeded storms (Mather et al. 1997; Bigg 1997).

Cooper et al. (1997) performed calculations using a parcel model to explore the effect of hygroscopic flare seeding on the initial size distribution of cloud droplets and on the subsequent evolution of that size distribution by coalescence. Their results showed that the growth of drops by the collision–coalescence process could be accelerated by seeding the cloud with the characteristic particle spectra produced by the hygroscopic flares.

In a complimentary study, Bigg (1997) independently analyzed the dataset of radar-measured properties such as storm mass and rain flux, collected in the South African field experiments. He suggested that the initiation of precipitation started at a lower height in the seeded clouds than in the unseeded ones. As a result, the falling precipitation particles in the seeded clouds were less dispersed by the wind shear and, therefore, produced a more concentrated downdraft closer to the updraft. The resulting surface gust front, therefore, was intensified, and its interaction with the storm inflow enhanced the convection.

Both Mather et al. (1997) and Bigg (1997) analyzed only radar-derived properties such as rain flux, storm mass, and area to evaluate the seeding effect. Although their results indicate increases in radar-derived properties, they do not address the issue of rainfall increases over the target area on the ground, which is the most important aspect for rain enhancement. In addition, mixed phase is the main characteristic of the summertime convective clouds, and a large part of the total rain amount from these clouds is attributed to the melting of ice particles, especially graupel particles. Although both in situ measurements (Mather et al. 1997) and theoretical calculations (Cooper et al. 1997) showed that the drop growth by coalescence could be accelerated by this new seeding approach, the response of ice-phase processes to the seeding is not understood fully. Therefore, it would be valuable to include ice microphysical processes in a model to evaluate and to understand the seeding effects properly. Furthermore, the dynamic effects proposed by Bigg (1997) also need to be explored further. With all these aspects considered, a multidimensional cloud model with detailed warm and cold microphysical processes is needed.

The aim of this paper is to evaluate the role of hygroscopic seeding with flares on the development of cloud and precipitation particles in mixed-phase convective clouds. For this purpose, a two-dimensional slab-symmetric cloud model with detailed warm and cold microphysics is used. Numerical experiments are conducted for clouds with different background cloud condensation nuclei (CCN) concentrations and spectra. The South African hypothesis is tested by introducing seeding particles below cloud base, with the full characteristic spectrum from the flares. In addition, the sensitivity of the development of precipitation particles to seeding parameters, such as seeding time, size of the seeding particles, seeding height, seeding amounts, and natural background CCN, is investigated. Comparisons are conducted between the seeded and unseeded clouds for the development of precipitation, size distributions of various species of hydrometeors, and radar reflectivity.

2. A brief description of the cloud model

The dynamic framework of the model was a two-dimensional slab-symmetric nonhydrostatic cloud model. The vertical and horizontal velocity were calculated based on the streamfunction and vorticity equation. The other predicting equations for virtual potential temperature, specific vapor perturbation, the specific concentration of CCN, and the specific mass and number of each species of hydrometeor considered (drops, graupel, ice crystals, and snowflakes) were based on the previous work by Reisin et al. (1996b) and Yin et al. (2000).

The warm microphysical processes included were nucleation of CCN, condensation and evaporation, collision–coalescence, and binary breakup (Low and List kernel). The ice microphysical processes included were ice nucleation (deposition, condensation freezing, contact nucleation, and immersion freezing), ice multiplication (Hallett–Mossop mechanism), deposition and sublimation of ice, ice–ice and ice–drop interactions (aggregation, accretion, and riming), melting of ice particles, and sedimentation of both drops and ice particles. All these microphysical processes were formulated and solved using the method of multimoments (Tzivion et al. 1987; Reisin et al. 1996b; Yin et al. 2000).

Three different types of ice were considered: ice crystals, graupel particles, and snowflakes (aggregates of ice crystals). Each particle type was divided into 34 bins with mass doubling in each bin. The masses of the lower boundary of the first bin and the upper boundary of the last bin for both liquid and solid phases were 0.1598×10^{-13} and $0.174\,68 \times 10^{-3}$ kg, which correspond to drop diameters of 3.125 and 8063 μm, respectively. The CCN spectrum was divided into 67 bins with a minimum radius of 0.0041 μm, and the seeding particles were divided into 35 bins with a minimum radius of 0.05 μm.

The coupling between dynamics and microphysics and the approach to determine supersaturation were similar to those of Reisin et al. (1996b). Using the values at time $t = t_0$ of horizontal and vertical velocity components u and w, virtual potential temperature θ_v, spe-

Unauthenticated | Downloaded 07/13/24 07:39 PM UTC

cific humidity q, specific concentration of CCN N_{CCN}, and mass and number concentrations of each species of hydrometeor in each bin M_{yk} and N_{yk} (where y represents any species of hydrometeor, and k is the bin number) the following procedure was adapted. 1) The turbulence parameter ν was calculated using the values of u and w at $t = t_0$. 2) The velocity components u and w at time $t = t_0 + \Delta t$ were determined from the streamfunction and vorticity equation. 3) A set of dummy values of θ_v^*, q^*, N_{CCN}^*, M_{yk}^*, N_{yk}^*, and temperature T^* were calculated at time $t = t_0 + \Delta t$ by taking account only of the dynamic terms (advection and turbulence) in the prognostic equations. 4) The saturation specific humidities with respect to water and ice corresponding to T^* were determined according to Teten's formula and the Clausius–Clapeyron equation, respectively. From these specific humidities, the supersaturations with respect to water and ice were found. 5) Nucleation processes of drops and ice particles were calculated based on the supersaturations calculated above. These processes were considered to occur instantaneously and to be time independent. After these calculations, the thermodynamic fields and number and mass concentrations of each species of hydrometeor were updated (at time t^{**}). The supersaturation was recalculated based on the new thermodynamic fields. 6) Condensation/evaporation, deposition/sublimation, collision–coalescence/breakup, and melting subsequently were calculated. The microphysical processes were applied simultaneously using the newly calculated functions (at time t^{**}). Last, the updated thermodynamic fields were calculated at time $t = t_0 + \Delta t$. The update of saturation specific humidity at time $t = t_0 + \Delta t$ was approximated by the first two terms of the Taylor expansion, resulting in consistency between the dynamic fields and the microphysics. 7) The ice multiplication process was calculated. 8) Sedimentation was calculated for all the number and mass concentrations of each species of hydrometeor.

The South African hypothesis (Mather et al. 1997; Cooper et al. 1997) was based on the fact that the seeding particles have the advantage over natural CCN by being larger in size and more soluble. According to this hypothesis, the growth of these particles would compete for the available water vapor with the natural CCN and prevent them from becoming activated. To simulate this effect of hygroscopic flare seeding properly, a separate spectrum of seeding particles was introduced. A dynamic equation for the specific concentration of the seeded particles was added into the above equations. In this way, two separate distributions of aerosols [1) natural and 2) seeded] were used. The nucleation of natural CCN and seeded particles was considered as follows.

The deliquescence of dry particles and the early growth of haze droplets below cloud base (defined as the altitude where relative humidity equals 100%) was not explicitly prognosticated. At each spatial point (x, z) and time t, initial droplets formed on dry particles were introduced into the calculations at their equilibrium size at 95% relative humidity for particles larger than 10 μm and at 100% relative humidity for particles smaller than 0.12 μm in radii. The equilibrium size for particles with sizes that fall in between was determined by interpolation. This assumption was made to provide some representation to the lag that would characterize the growth of the largest CCN while keeping unaffected the growth of the small CCN (e.g., Mordy 1959; Cooper et al. 1997). Because of the difference in their chemical compositions, seeding particles become aqueous solution earlier than do natural CCN of the same size.

Further condensation growth or evaporation of these newly born droplets was calculated by analytically solving the kinetic diffusion equation in one time step based on the multimoments method (Tzivion et al. 1989; Reisin et al. 1996b). This method allows the supersaturation to change within the time step, and therefore it particularly is accurate when a relatively long time step is used.

The grid size of the model was set to 300 m in both the horizontal and vertical directions (separate numerical tests using grid sizes of 150 and 200 m showed that, except for a 2-min delay in the cloud and rain initiation, the development of cloud properties such as liquid water content, maximum updraft, and ice content were similar to those reported in this paper). The width and height of the domain were 30 and 12 km, respectively. The time step for all the processes was 5 s except for diffusive growth/evaporation, for which a shorter time step of up to 2.5 s was used.

3. The initial conditions and seeding material

a. The thermodynamic conditions

In this paper, a single-cell cloud with large instability was considered to be representative of one of the growing cells in a convection complex, such as those commonly encountered in summertime storms. The tests presented here mainly concentrate on how the hygroscopic seeding from flares influences the microphysical structure of the cloud and the precipitation. A theoretical thermodynamic profile (Fig. 1) that produced a cloud with cloud base at 8°–10°C and top at −25°C was used to represent the average initial thermodynamic conditions of the summer convective clouds (e.g., Krauss et al. 1987; Cooper and Lawson 1984). To initiate the cloud, a temperature perturbation of 2 K was applied for one time step at $t = 0$ at a height of 600 m, in the middle of the domain.

b. The natural CCN

The initial activity distribution of natural CCN was expressed as a function of supersaturation,

$$N(S) = N_0(S/S_0)^k. \quad (1)$$

Here $N(S)$ is the cumulative number of CCN active at

Unauthenticated | Downloaded 07/13/24 07:39 PM UTC

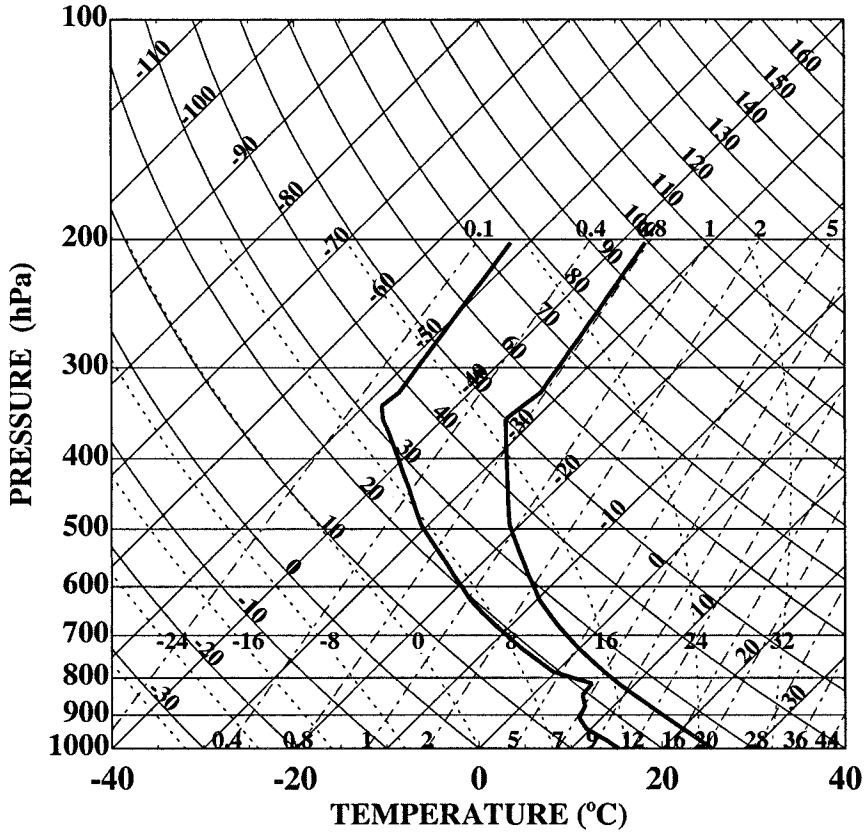

FIG. 1. Vertical profiles of temperature and dewpoint used in the current work.

or below the supersaturation S, and S_0 is the reference supersaturation (1%) at which the cumulative concentration equals N_0. In this paper the values of N_0 and coefficient k representing continental clouds (hereinafter, cloud C) were determined based on Cooper et al. (1997). The CCN spectrum was divided into three ranges, and the values of N_0 and k for each are given in Table 1.

This CCN spectrum was applied to the main simulations. To test the sensitivity of seeding to variation in natural CCN, other CCN spectra also were considered. For a maritime cloud (cloud M), the values $N_0 = 100$ cm^{-3} and $k = 0.7$, based on the Twomey and Wojciechowski (1969) measurements, were used. In addition, CCN spectra with N_0 equal to 600 and 400 cm^{-3} and $k = 0.5$, based on Reisin et al. (1996a) and Cooper et al. (1997), were selected to represent a moderate continental cloud (MC) and an intermediate cloud (IM) between continental and maritime, respectively.

TABLE 1. Values of N_0 and k in Eq. (1) used in simulations of the continental cloud (see text for explanation).

Supersaturation (%)	N_0 (cm^{-3})	k
$S \geq 0.4$	1000	0.5
$0.007 \leq S < 0.4$	4000	2
$S < 0.007$	6.62×10^7	4

The CCN concentrations were assumed to decrease exponentially with altitude with a scale height of 2.5 km [according to Pruppacher and Klett (1997)]. The above CCN spectra, therefore, produced CCN concentrations of 800, 500, 300, and 100 cm^{-3} (active at 1% supersaturation), respectively, for the continental, moderate continental, intermediate, and maritime cloud at cloud-base level. The CCN distributions for all these clouds are shown in Fig. 2, and the particles were assumed to be composed of ammonium sulfate. This assumption was based on the previous studies (e.g., Fitzgerald 1974; Takeda and Kuba 1982) that showed that the differences in the chemical composition of CCN [such as NaCl, and $(NH_4)_2SO_4$] do not significantly change the predicted size distribution of cloud droplets.

c. The distribution of seeding particles

Mather et al. (1997) determined the size distribution of the seeding particles by measuring them 50 m behind the seeding aircraft. These data can be described with a trimodal lognormal distribution as suggested by Cooper et al. (1997),

$$\frac{dN}{d\ \ln r_n} = \sum_{i=1}^{3} \frac{n_i}{(2\pi)^{1/2}\ \log\sigma_i\ \ln 10} \exp\left\{-\frac{[\log(r_n/R_i)]^2}{2(\log\sigma_i)^2}\right\}, \tag{2}$$

Unauthenticated | Downloaded 07/13/24 07:39 PM UTC

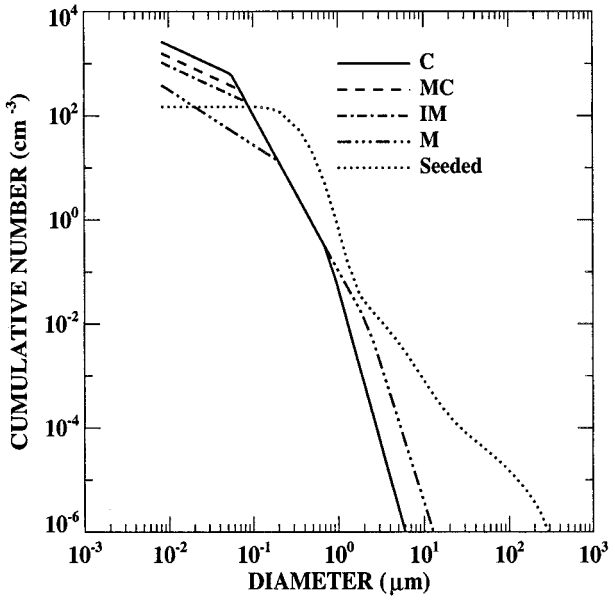

FIG. 2. Distributions of initial CCN and seeded particles from the flares. See text for a more detailed explanation.

where, r_n, n_i, R_i, and σ_i are the radius of the particle, the total number concentration, geometric mean radius, and geometric standard deviation for each mode, respectively, and the subscript $i = 1$, 2, or 3 represents the three modes. As used here, the three distributions have respective geometric mean radii of 0.15, 0.5, and 5 μm and geometric standard deviations (relative to log base 10) of 0.2, 0.4, and 0.6. The ratio of the concentrations for the three lognormal distributions was 1:7.0 $\times 10^{-4}$:2.3 $\times 10^{-6}$, which was based on Fig. 1 of Cooper et al. (1997). All the seeding particles were assumed to be potassium chloride, which is the primary constituent in the smoke produced by the flares. The full spectrum of the seeding particles used in this study is shown in Fig. 2 (dotted line).

4. Results

a. Simulation of the reference cases

A summary of the maximum values obtained for the four reference (unseeded) clouds is presented in Table 2. The evolution of the maximum updraft, liquid water content (LWC), and concentration of drops in the middle of the clouds is shown in Fig. 3. The general features of the macrostructure of these clouds at the developing stage were similar; cloud droplets began to appear after 23 min of simulation and rapidly reached their maximum concentrations about 14 min later. The maximum updraft remained small (less than 2 m s^{-1}) until 28 min; thereafter, the clouds experienced a rapid developing phase and reached their peak value, 13 m s^{-1}, at the height of 4 km after 44 min of simulation. The maximum LWC of these clouds, 4.3 g kg^{-1}, was achieved at a height of 4.8 km after 45 min. Cloud base, defined as the altitude at which the relative humidity began to exceed 100%, was at 1.5–1.8 km, and cloud top was at 6.6 km above the ground. The width of the main updraft at cloud base was about 1.2 km.

TABLE 2. Maximum values of the four unseeded clouds: maritime (M), intermediate (IM), moderate continental (MC), and continental (C).

Parameters	M	IM	MC	C
Updraft speed (m s^{-1})	13.3	13.0	12.8	12.6
Water content (g kg^{-1})				
Liquid water	4.26	4.26	4.29	4.37
Ice crystals	0.68	0.57	0.64	1.0
Graupel particles	4.49	2.80	2.22	1.54
Drops $\geq$ 1 mm in diameter	2.85	1.46	0.92	0.35
Drops $\geq$ 4 mm in diameter	0.11	0.10	0.07	0.0
Graupel $\geq$ 1 mm in diameter	4.49	2.80	2.20	1.51
Graupel $\geq$ 4 mm in diameter	4.36	2.01	1.35	0.44
Number concentration				
Drops (cm^{-3})	111	374	557	860
Ice crystals (L^{-1})	30.4	40.5	58.6	64.0
Graupel particles (L^{-1})	3.77	4.12	3.51	2.05
Drops $\geq$ 1 mm in diameter (L^{-1})	1.73	1.15	0.81	0.21
Drops $\geq$ 4 mm in diameter (m^{-3})	1.77	1.46	1.08	0.01
Graupel $\geq$ 1 mm in diameter (L^{-1})	0.75	0.87	0.81	0.65
Graupel $\geq$ 4 mm in diameter (m^{-3})	54.8	40.9	30.3	13.5
Maximum radar reflectivity (dBZ)	66.3	62.0	57.8	50.1
Time of rain initiation (min)	47	51	53	55
Maximum rain rate (mm h^{-1})	158.3	72.9	41.9	8.2
Maximum accumulated rain (mm)	20.5	9.1	5.0	1.0
Integrated rain amount (m^3)	24 858	14 388	8478	2985

Significant differences were observed in the development of precipitation particles, radar reflectivity, rainfall rate, and rain amount in these clouds, as seen in Table 2. The specific mass and concentration of millimeter-size drops and graupel particles, the radar reflectivity, and the rainfall rate all developed faster and achieved higher values in the maritime cloud (M) than in the other clouds.

In the maritime cloud (case M), the collision–coalescence of drops was sufficient for efficient production of rain. Graupel was formed by collisions between big drops and ice crystals and by self-freezing of big drops and reached high mass content (maximum of 4.5 g kg^{-1}). Riming (collection of small drops by larger ice crystals) was scarce, because the drops and the ice crystals were of similar size. Rain began 47 min from model initiation and reached a maximum rainfall rate of 158

Unauthenticated | Downloaded 07/13/24 07:39 PM UTC

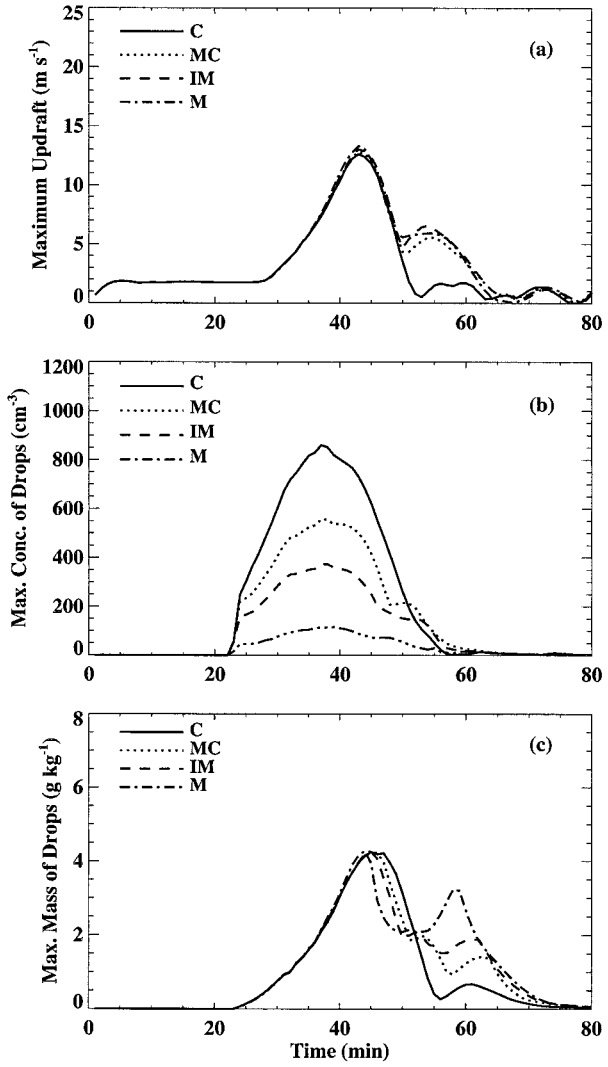

FIG. 3. Maximum values of (a) updraft speed, (b) droplet concentration, and (c) LWC at the middle axis as a function of time in clouds formed on different CCN spectra.

mm h^{-1}. The maximum accumulated rain on the ground was 20 mm and the integrated rain amount (by assuming that the cloud extends 1 km in the *y*, or cross, direction) was 25 metric kilotons.

In the continental cloud (case C), the growth of the raindrops by the collision–coalescence process was much less efficient. Ice processes played a more significant role in the development of precipitation, and rain resulted primarily from graupel particles produced by riming. The maximum mass of graupel was 1.5 g kg^{-1}, much less than in the maritime case. The maximum radar reflectivity was 50 dB*Z*, in comparison with 66, 62, and 58 in cases M, IM, and MC, respectively. Rain was initiated 8 min later than in the maritime cloud (22 min from cloud initiation) and lasted only 20 min. The rainfall rate was considerably lower, and the rain amount was reduced, with a maximum accumulated rain of only 1 mm and integrated rain amount of 3 metric kilotons.

The development of precipitation particles, radar reflectivity, rainfall rate, and rain amount in clouds MC and IM fell between that of cases C and M. These results show that, with the CCN concentration and spectrum changing from maritime to continental, the cloud became a less-efficient rain producer, although the maximum LWC condensed from the vapor was similar. This result also implies that a larger potential exists in the continental clouds for augmenting rain production by artificial seeding.

b. Simulation of seeding experiments

More than 40 model seeding experiments were conducted to test the South African hypothesis and to investigate the sensitivity of the development of precipitation to seeding parameters such as seeding time, particle size from the flares, seeding height, and seeding amounts. The additional CCN for the seeding experiments were introduced over a 4-min period to be consistent with the burning time of the flares (Bruintjes 1998, personal communication). The seeding experiments discussed in the following sections were conducted mainly within the 1.2-km main updraft region. Because the present model is 2D and dispersion of particles needs to be done in mass (or number of particles) per unit volume, seeding was done along the *x* axis (1.2 km) allowing the particles to fill a box 300 m high and 300 m in the *y* direction. The amount of seeding material was about 2 kilograms per minute, or 8 kilograms per seeding. This amount is equivalent to what has been used in the South African field experiments.

The seeding parameters and the differences between the seeded and unseeded cases in accumulated rain at the middle of the domain ΔR_{ac}, the integrated rain amount on the ground ΔR_{int}, and rain initiation time for 30 cases are summarized in Table 3.

1) TIME OF SEEDING

In the first group of experiments, 150 cm^{-3} hygroscopic particles with the full characteristic distribution from the flares (Fig. 2), as used in the South African experiments, were introduced below cloud base (1.5 km) within the main updraft region but at different times. These experiments were designed to find the optimal seeding time for a newly formed convective cell and to test the South African hypothesis.

The main results for five runs (C1–C5) in the continental cloud (C) are listed in Table 3. It is seen that positive seeding effects were obtained when seeding was conducted before the cloud reached its maximum development (44 min of simulation, or 21 min after cloud initiation). Maximum rain enhancement (18% of integrated rain amount and 125% of accumulated rain at the middle of the domain) was achieved when seeding

Unauthenticated | Downloaded 07/13/24 07:39 PM UTC

TABLE 3. Seeding parameters and differences between the seeded and unseeded clouds in accumulated rain at the middle of domain ΔR_{ac}, integrated rain amount ΔR_{int}, and time of rain intiation T_r.

Case	Particle size (μm)	Seeding amounts	Time (min)	Height (km)	ΔR_{ac} (%)	ΔR_{int} (%)	T_r (min)
C1	Full	150 cm^{-3}	2–6	1.5	96.1	8.6	45
C2	Full	150 cm^{-3}	6–10	1.5	125.2	17.9	45
C3	Full	150 cm^{-3}	10–14	1.5	72.8	11.7	47
C4	Full	150 cm^{-3}	14–18	1.5	14.6	0.7	49
C5	Full	150 cm^{-3}	18–22	1.5	0.0	−0.4	55
C6	$1 \le r \le 10$	26.7 L^{-1}	6–10	1.5	0.0	0.1	55
C7	$r \ge 10$	0.16 L^{-1}	6–10	1.5	136.9	33.7	45
C8	$r \le 1$	150 cm^{-3}	6–10	1.5	−12.6	−17.1	55
C9	Full	150 cm^{-3}	6–10	1.8	204.9	29.8	43
C10	Full	150 cm^{-3}	6–10	2.1	255.3	40.4	42
C11	$r \ge 10$	0.16 L^{-1}	6–10	2.1	288.4	66.3	42
C12	Full	750 cm^{-3}	6–10	1.5	337.9	48.5	41
C13	Full	1500 cm^{-3}	6–10	1.5	508.7	89.7	41
C14	$r \ge 10$	1.6 L^{-1}	6–10	1.5	592.2	162.1	41
C15	$1 \le r \le 10$	2.67 cm^{-3}	6–10	1.8	149.5	107.5	51
C16	$r \ge 10$	0.45 L^{-1}	6–10	1.8	546.5	131.5	40
MC1	Full	150 cm^{-3}	2–6	1.5	−1.0	−16.0	45
MC2	Full	150 cm^{-3}	6–10	1.5	−1.2	−15.8	45
MC3	Full	150 cm^{-3}	10–14	1.5	−2.4	−9.2	47
MC4	Full	150 cm^{-3}	14–18	1.5	−7.0	−5.9	50
MC5	Full	150 cm^{-3}	18–22	1.5	−2.6	−1.6	53
MC6	$1 \le r \le 10$	26.7 L^{-1}	6–10	1.5	0.0	0.1	53
MC7	$r \ge 10$	0.16 L^{-1}	6–10	1.5	31.9	4.3	45
MC8	$r \le 1$	150 cm^{-3}	6–10	1.5	−29.7	−22.2	53
IM1	Full	150 cm^{-3}	6–10	1.5	3.0	−12.1	45
IM2	$r \ge 10$	0.16 L^{-1}	6–10	1.5	14.1	0.3	45
M1	Full	150 cm^{-3}	6–10	1.5	−3.7	−3.4	45
M2	$r \ge 10$	0.16 L^{-1}	6–10	1.5	2.8	0.0	45

material was introduced at 29–33 min of simulation, or 6–10 min after cloud initiation (C2). This optimal time range corresponded to the stage at which the clouds began their rapid development. Either seeding before or after this time led to lesser rain enhancement.

Figure 4 shows the droplet size distribution after 36 min of simulation (13 min after cloud initiation) in the unseeded (hereinafter, C0) and seeded cases (C2) for the continental cloud. The figure shows that seeding with the particle spectrum from the flares led to a broader droplet size distribution. This result is especially clear in the distribution function of water content (left panel). The concentration of the drops larger than 100 μm in diameter was 0.21 L^{-1} in case C2, but in case C0 no droplet larger than 100 μm was observed. The drizzle-size droplets and raindrop embryos grown on the larger artificial CCN triggered the growth of drops by collision and coalescence, which, in turn, influenced the formation and evolution of ice-phase hydrometeors in the clouds, as will be discussed later.

The seeding-induced changes in the size distribution of the precipitation particles led to significant changes in the development of the radar reflectivity, because the latter is very sensitive to particle size ($\propto D^6$; D is diameter). Figure 5 shows the development of radar reflectivity in case C2 and in the unseeded case (C0) as a function of time. From this figure, one can see that the radar reflectivity appeared earlier and at a lower altitude in case C2 than in C0, and the peak value was higher in the former case than in the latter. In the above discussion, it was shown that the best time for seeding this kind of cloud is 6–10 min after cloud initiation. This time corresponds to the stage in which the cloud began its rapid developing phase. It is noted in Fig. 5 that the radar reflectivity at this time is much lower than 0 dBZ, implying that, for best results, seeding should be conducted before the cloud produces a detectable echo on a typical weather radar.

Figure 6 shows the rainfall rate on the ground as a function of time in cases C0 and C2. In case C0, rain started after 55 min of simulation near 0.9 km away from the middle of the cloud and reached a maximum rain rate of 8.2 mm h^{-1} 7 min later. In case C2, however, rain was initiated 10 min earlier than in the unseeded case near the middle region under the cloud and reached a peak rain rate of 18.2 mm h^{-1} at 57 min. Although

Unauthenticated | Downloaded 07/13/24 07:39 PM UTC

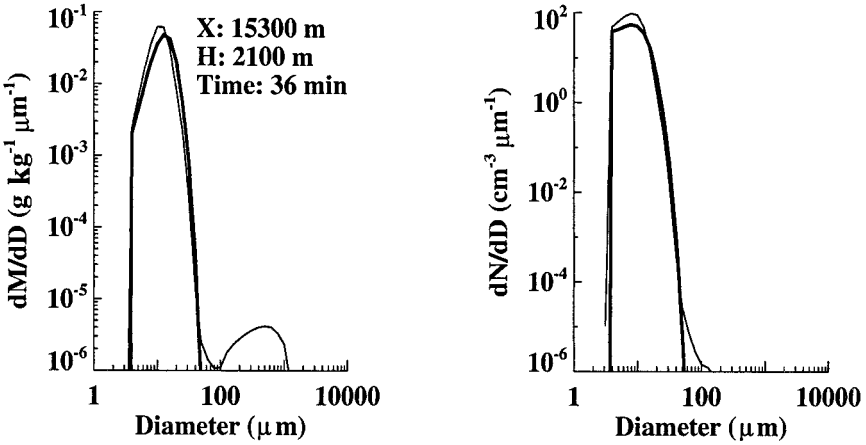

FIG. 4. Drop mass (left) and concentration (right) distributions for the unseeded case C0 (thick line) and seeded case C2 (thin line) after 36 min of simulation. The location is shown above the curves.

the region where rain fell was a little wider in the unseeded case than in the seeded one, the larger rainfall rate in the seeded case resulted in larger integrated rain amount on the ground (Table 3).

2) SIZE OF THE SEEDING PARTICLES

Cases C6–C9 were carried out to test the sensitivity of rain production to the size of seeding particles and the relative importance of different size segments of the particles from the flares. In these cases, the particle spectrum from the flares was divided into the following size segments: $r \leq 1$, $1 \leq r \leq 10$, and $r \geq 10$ μm. Here, r is the radius of the dry particles. The concentrations of these segments in a spectrum with total concentration of 150 cm^{-3} were ~150, 26.7, and 0.16 L^{-1}, respectively, and the mass allocations were 39%, 3%, and 58%, respectively. It can be seen that most of the particles (more than 99%) produced by the flares are smaller than 1 μm, but the fewer giant particles in the tail of the distribution account for a large fraction of the mass.

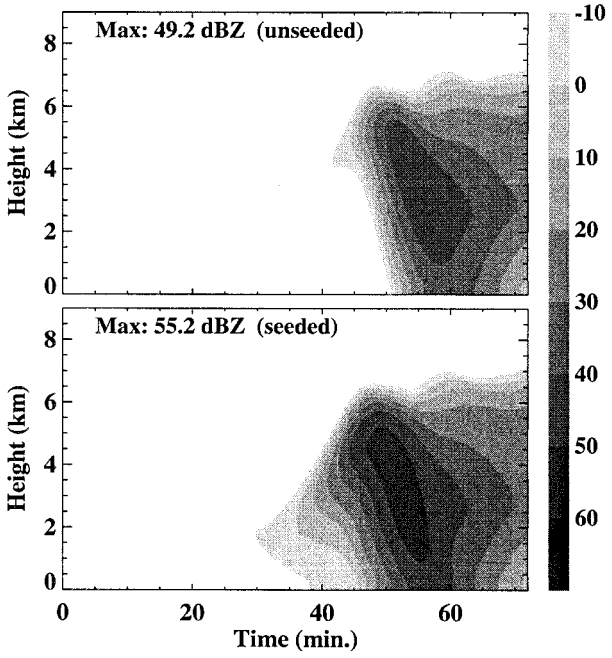

FIG. 5. Radar reflectivity at the cloud middle as a function of time in the unseeded case (top) and seeded case C2 (bottom) for the continental cloud.

Seeding experiments were conducted using only a certain segment of the seeding spectrum, and the particles were introduced below the cloud base 6–10 min after cloud initiation. From the results presented in Table 3, it is clear that, out of the full particle spectrum produced by the flares, the most beneficial particles for rain enhancement were those larger than 10 μm in radius (C7). Introduction of these large particles promoted the formation of drizzle-size droplets and raindrop embryos by nucleation and condensation processes. Although these solution droplets might never have reached their critical sizes by diffusional growth, they could grow rapidly by collecting other smaller droplets. This method of growth can be seen from the differences in the development of millimeter-size raindrops between the seeded and unseeded cases shown in Fig. 7.

In Fig. 7, the maximum values of water content and concentration of raindrops with diameters larger than 1 and 4 mm are shown as a function of time. Seeding experiments using the full particle spectrum from the flares or only those particles larger than 10μm both led to earlier development and larger numbers of millimeter-sized raindrops than in the unseeded case. This result was especially true for drops larger than 4 mm, which were absent in the unseeded case but reached a maximum concentration of 1 m^{-3} in the seeded cases. From Fig. 7, it can be seen again that seeding with only giant

Unauthenticated | Downloaded 07/13/24 07:39 PM UTC

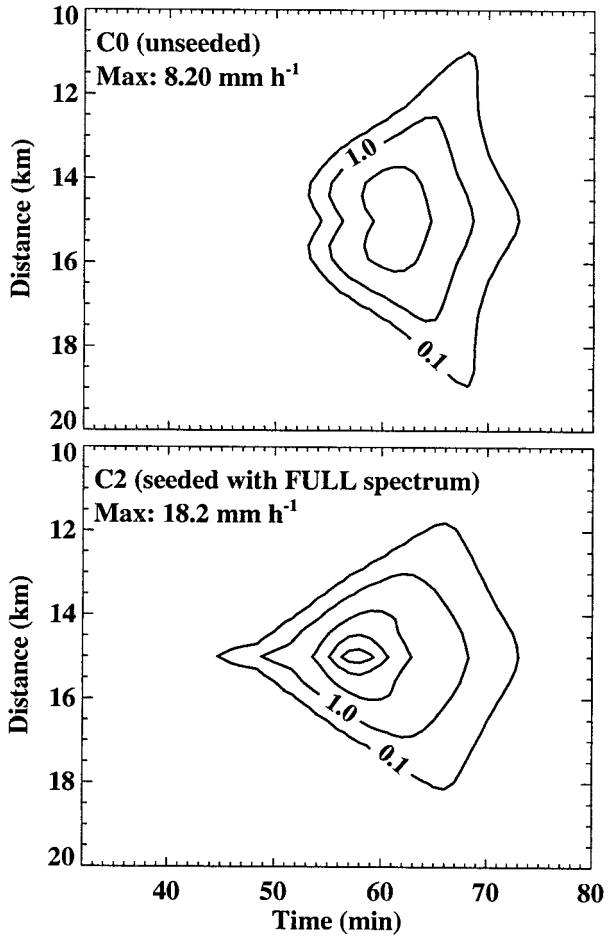

FIG. 6. Rainfall rate on the ground as a function of time in the unseeded case (top) and seeded case (C2; bottom). The contours are 0.1, 1, 5, 10, 15 mm h^{-1}.

particles from the flares produced more raindrops than when the full spectrum was used.

The results in case C8 indicate that seeding using only particles smaller than 1 μm produced a negative effect. This result is because the sizes of the small seeded particles were similar to that of the natural CCN. Their dispersal into the cloud only increased the total droplet concentration and reduced the efficiency of rain development. It is noted that the rain enhancement produced by seeding with a full spectrum (125% in accumulated rain and 18% in integrated rain amount) is roughly the sum of the positive effect obtained by seeding with particles larger than 10 μm (137% in accumulated rain and 34% in integrated rain amount) and the negative effect by the submicron particles (-13% in accumulated and -17% in integrated rain amount). The relative contributions from these two subranges of seeding particles depend on the effectiveness of the natural CCN spectra. It will be seen in a later section that in more-maritime clouds the negative effect produced by the submicron particles exceeds the positive effect produced by larger particles, leading to a net negative effect.

The results in Table 3 also show that seeding with particles in the range from 1 to 10 μm only produced a negligible effect. This result is expected, because the mass distributed in this segment is much smaller than that of particles larger than 10 μm. The seeding experiments were repeated using the same mass for both the segment of particles in the range of 1–10 μm and the segment larger than 10 μm. The results for these two tests are shown in Table 3 as C15 and C16. Comparison of these two experiments indicates that both produced significant enhancement of the integrated rain amount at the ground. It is noted also that seeding with larger particles (>10 μm) resulted in much more intensive rain under the center of the cloud than did seeding with particles ranging from 1 to 10 μm, and the time of rain initiation was earlier in the former case than in the latter.

A comparison between the cloud droplet distributions at cloud base in the unseeded case C0 and the seeded cases C15 and C16 1 min after seeding was completed is shown in Figs. 8a,b. In these figures, the concentrations of drops larger than 40 μm in diameter in C15 and C16 are, respectively, 9 and 0.2 L^{-1}, but in C0 there are no such large drops. It indicates again that seeding led to broader drop size distributions at cloud base. The difference between cases C15 and C16 is that most of the large drops in C15 are in the range of 40–100 μm, whereas more drops with diameter larger than 100 μm are observed in C16. This difference implies that the droplets in the former case needed more time to grow to raindrops than did the latter.

The droplet concentrations at cloud base in the unseeded case C0 and some of the seeded cases are given in Table 4. These results indicate that seeding with particles larger than 10 μm (C7 and C14) prevented some of the natural CCN from becoming activated and resulted in reduction of the cloud droplet concentration. On the other hand, when only smaller particles ($r < 1$ μm; C8) were used, the total drop concentration actually increased. This increase was due to the fact that some of the natural CCN were in fact larger and more effective than the seeded ones. As a result, both natural and seeded particles became activated, leading to higher droplet concentration. When the full spectrum from flares was introduced (C2), the larger seeded particles became activated first, but, because there was still moisture left for other particles to form drops, both seeded and natural nuclei became activated. In other words, this case is similar to but milder than C8.

3) SEEDING HEIGHT

Cases C9 and C10 were carried out with the same particle sizes and concentrations as in case C2, but the heights of seeding were different. In C9 and C10 the seeding material was introduced at 1.8 (near cloud base)

Unauthenticated | Downloaded 07/13/24 07:39 PM UTC

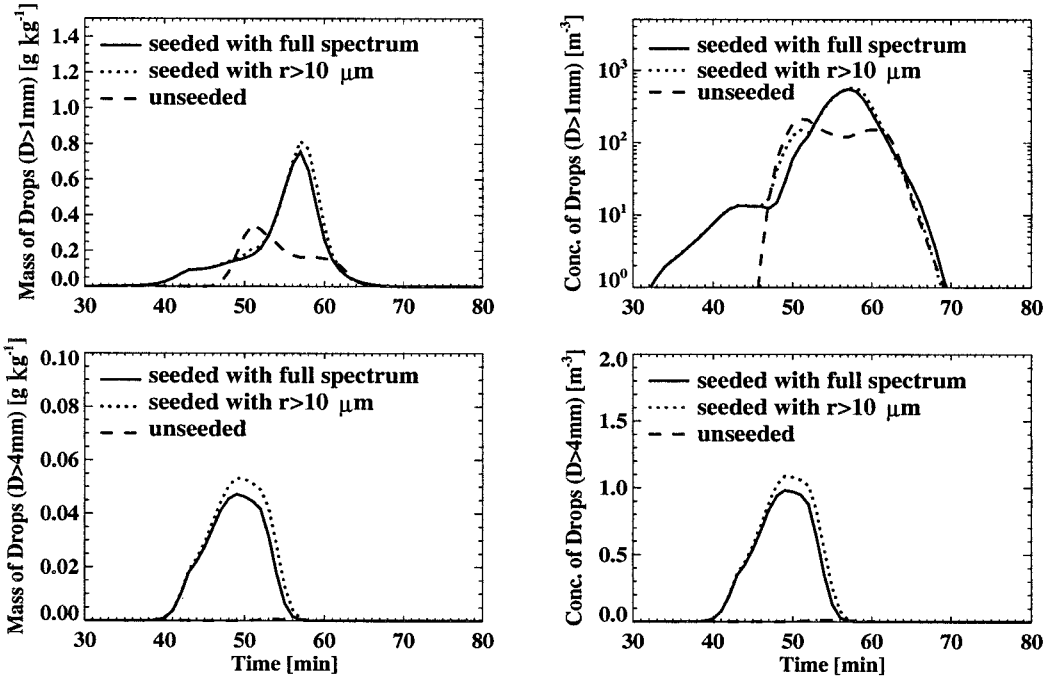

FIG. 7. Maximum values of water content (left) and concentration (right) of the raindrops with diameter larger than 1 (top) and 4 mm (bottom), respectively, in the unseeded case (dashed line), the case seeded with the full spectrum of particles from the flares (solid line), and the case seeded with only particles larger than 10 μm (dotted line).

and 2.1 km, respectively. Comparison of these two cases with C2 reveals that seeding at 2.1 km produced twice as much rain enhancement as that at 1.5 km (Table 3). Similar results also were obtained when seeding was conducted using only the giant particles (compare C11 with C7). These results mean that the best effect is obtained when seeding is conducted inside the cloud instead of below cloud base. The reason for this conclusion is attributed to the effects of dilution, which reduces the concentration of seeding particles that actually make it into the cloud from their injection level below cloud base.

4) SEEDING AMOUNTS

A comparison of cases C12 and C13 with C2 reveals that the seeding effect became more pronounced with an increase in the seeding amounts. Rain enhancements of 49% and 90% were achieved in C12 and C13, respectively, much higher than that in C2 (18%). This result was especially true when seeding was carried out using only the large particles (compare C14 with C7). Considering the limitation of the tools for dispersion used in the field, it seems that overseeding is not a problem with which to be concerned when using hygroscopic material from flares. Comparison of the results between C12 and C10 (the amount of seeding material in C12 was 5 times that in C10, but the seeding height in C10 was 2.1 km) indicates that the rain increase by seeding with one flare inside the cloud is equivalent to seeding with 4–5 flares below cloud base.

c. Sensitivity to natural CCN spectra

In the above tests, seeding experiments were carried out in a continental cloud (C) with natural CCN concentration of about 800 cm^{-3} at 1% supersaturation. Because of the differences in the efficiency of development of precipitation in different clouds, the optimal seeding parameters obtained in case C are not necessarily the same for other clouds that have different CCN spectra. For this purpose, seeding experiments also were conducted for clouds with lower CCN concentration (MC and IM) and wider distribution (M).

The results obtained for cloud MC are listed in Table 3 (MC1–MC5). In these cases, 150 cm^{-3} seeding particles with the full spectrum from the flares were introduced below cloud base at different times. The results indicate that seeding this kind of cloud (also in clouds IM and M, not shown) with the full spectrum from the flares only produced marginal or negative effects on the precipitation (Table 3). Furthermore, no preferred seeding time was found, although rain started earlier in comparison with the unseeded cases. As has been shown in the last section, the most effective seeding particles in the spectrum responsible for rain initiation were those larger than 10 μm. On the other hand, the submicron particles, which account for more than 99% of the total

Unauthenticated | Downloaded 07/13/24 07:39 PM UTC

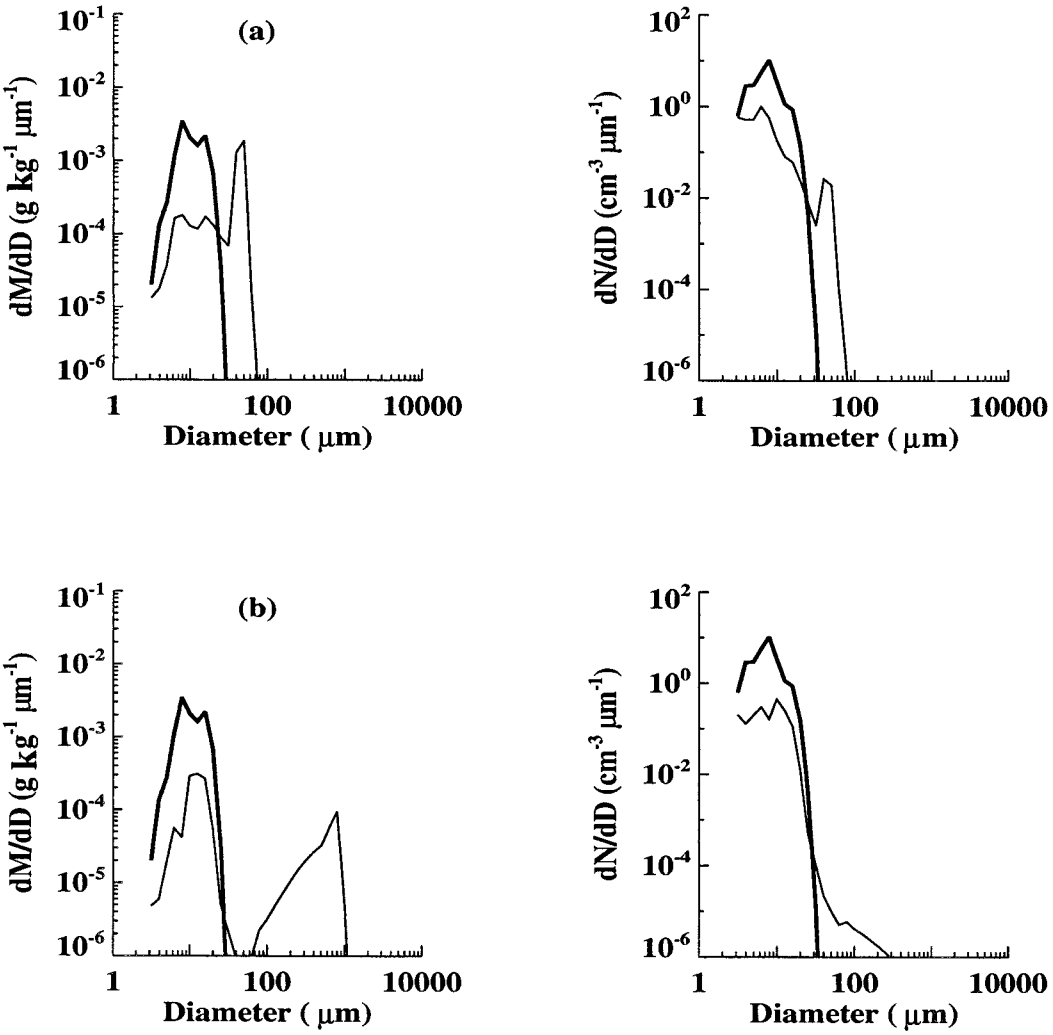

FIG. 8. Droplet mass and concentration distributions at cloud base for the unseeded case (thick line) and seeded case (thin line), 1 min after completing seeding. (a) C0 vs C15; (b) C0 vs C16.

number emitted from the flares, always produced negative effects for rain production. The net effect of seeding with the full characteristic distribution from the flares, therefore, is dependent on the relative contributions of these two parts, which are, in turn, determined by the natural CCN. In this case (MC), seeding with the submicron particles (MC8 in Table 3) reduced the integrated rain amount by 22%, much larger than the positive effect (4%) produced by the giant particles (MC7). Therefore, seeding with the full spectrum resulted in a net negative effect on the rain production, and no favorable time window for seeding was found. The experiments were repeated using only the particles larger than 10 μm but seeding at different times. The best seeding time for rain enhancement was between 6 and 10 min after cloud initiation (not shown) as was the case in other experiments discussed in previous sections. This result is because the phase of the development of all these clouds was similar and depended only on the initial thermodynamic conditions.

TABLE 4. Droplet concentrations (cm^{-3}) at cloud base 3 min after seeding was completed in some of the seeded cases and the reference case C0.

Case	C0	C2	C6	C7	C8	C14
Concentration	340	351	340	314	422	295

Figure 9 shows the differences in integrated rain amount between the seeded and unseeded clouds with different natural CCN concentrations and spectra. In this case 0.16 L^{-1} seeding particles with radii larger than 10 μm were introduced 300 m below and above cloud base. From this figure one can see that the effect produced by seeding decreased as the natural CCN spectrum changed from continental to maritime. The rain production in a maritime cloud cannot be increased by hy-

Unauthenticated | Downloaded 07/13/24 07:39 PM UTC

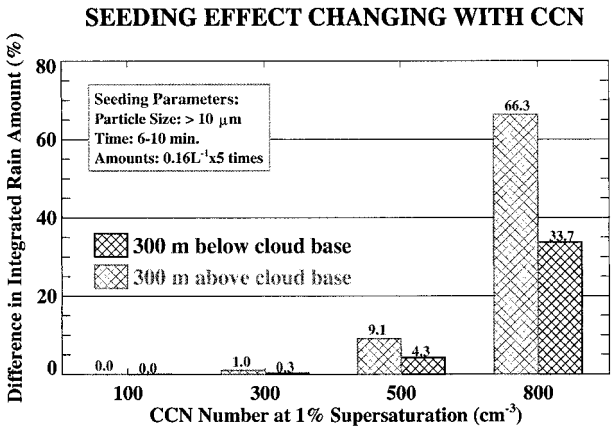

FIG. 9. Differences in integrated rain amount between the seeded and unseeded cases for clouds with different natural CCN.

groscopic seeding, because the natural development of precipitation in this type of cloud already is very efficient (Table 2). In continental clouds, on the other hand, the growth of raindrops by collision–coalescence is limited, because higher concentrations and smaller-size droplets are formed on more CCN particles. Therefore, the potential for rain enhancement is much greater.

5. Discussion

The results obtained here support the hypotheses that the larger artificial CCN provided by flares would influence the initial condensation process in the cloud, resulting in a broader droplet spectrum at an early stage of the cloud's lifetime and in the acceleration of precipitation growth by the coalescence process. These results are consistent with the measurements by Mather et al. (1997) and the theoretical calculations by Cooper et al. (1997).

In mixed-phase clouds, a large part of the precipitation is produced via drop–ice interactions. Because seeding with hygroscopic particles changes the growth rate of the drops, it also influences the drop–ice interactions and the production of ice particles. Figure 10 shows the maximum values of water content and concentration of graupel particles with a diameter larger than 1 and 4 mm as a function of time in the same cases shown in Fig. 7. It is clear that seeding not only accelerated the growth of raindrops but also promoted the development of ice-phase precipitation particles. This result is because the processes of drop freezing are very sensitive to the drop size distribution. The large drops that form early in the cloud have a higher probability of freezing than do the smaller ones. Also, because of their higher collection efficiency, more small droplets are captured, leading to faster growth of graupel particles. Therefore, a large part of the increased precipitation in convective cloud by hygroscopic seeding could be attributed to the enhanced graupel production.

It is interesting to note from Fig. 10 that seeding did not increase the maximum water content and concentration of all the graupel particles but led to a larger number of large particles. This finding is verified by the

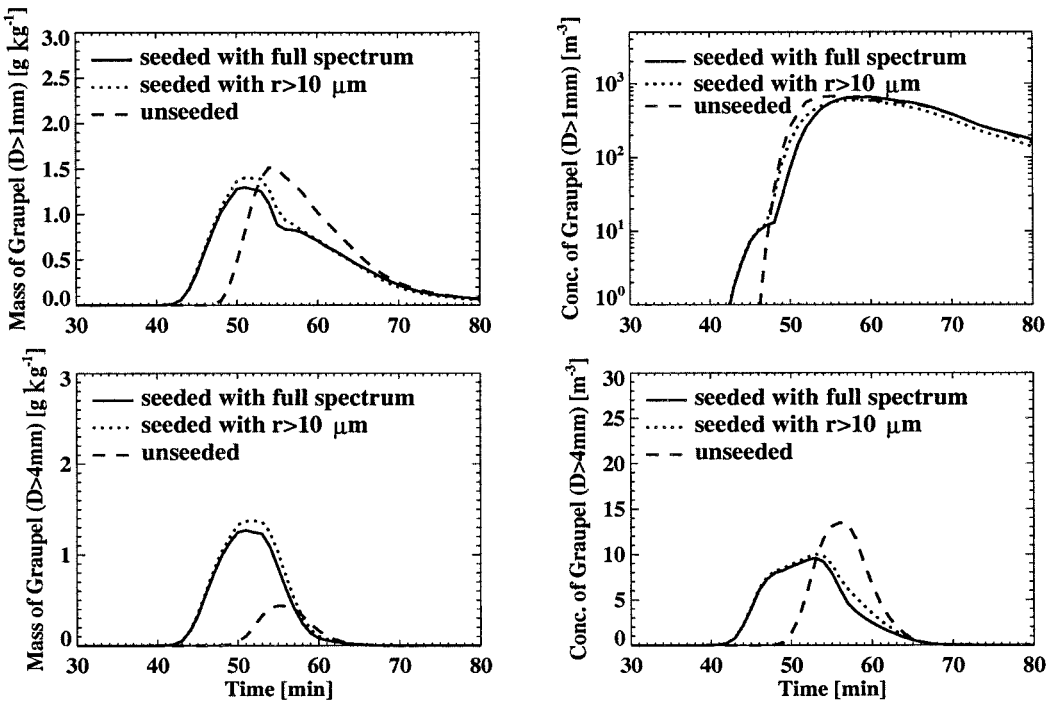

FIG. 10. Similar to Fig. 7 but for graupel particles.

Unauthenticated | Downloaded 07/13/24 07:39 PM UTC

larger water content and lower concentration of particles with sizes larger than 4 mm in diameter.

6. Conclusions

Numerical simulations were conducted for a specific initial thermodynamic profile. Although more experiments are needed to draw more general conclusions, the results from the above numerical experiments could be used as a guide for some field operations. From these results one can conclude the following.

1) The results of the numerical experiments confirm the hypothesis of Mather et al. (1997) that using flares for seeding hygroscopic particles below cloud base could lead to a broadening of the cloud drop spectrum, an earlier formation of raindrops, graupel particles, and radar reflectivity at a lower altitude. It does not confirm, however, the idea that the droplet concentration at cloud base will be reduced by seeding particles with the full spectrum from the flares.
2) Seeding with the full particle spectrum from the flares could increase rainfall amount in continental clouds with CCN concentration of more than about 500 cm^{-3} (at 1% supersaturation). Seeding more-maritime clouds resulted in reduction of the total rain, although the rain formation was accelerated in some cases.
3) Out of the full spectrum of seeding particles, the most effective particles were those with radii larger than 1 μm, especially those larger than 10 μm; the particles smaller than 1 μm always had a negative effect on the rain development.
4) Although seeding below cloud base resulted in rain enhancement, seeding above cloud base was found to be more effective. It was found that seeding with four flares below cloud base produced about the same results as using only one flare above cloud base.
5) The best seeding effect was obtained when seeding was conducted a few minutes after cloud initiation. The radar reflectivity at that time period was usually lower than 0 dBZ. Rain enhancement also increased with the concentration of large seeding particles (at least for the amounts tested here).

These conclusions may be used as guidelines in field experiments. One should keep in mind, however, the limitations of the model, which include, among others, the 2D dynamics, limited spatial resolution, and simplifications associated with the nucleation process.

Acknowledgments. We thank the Israel Water Commissioner for partially funding this research. Thanks are also due to Mr. and the late Mrs. L. Ross for their contributions to the laboratory, which made part of this work possible. Part of the calculations were conducted on the Cray J932 of IUCC of Israel.

REFERENCES

Bigg, E. K., 1997: An independent evaluation of a South African hygroscopic cloud seeding experiment, 1991–1995. *Atmos. Res.,* **43,** 111–127.

Biswas, K. R., and A. S. Dennis, 1971: Formation of a rain shower by salt seeding. *J. Appl. Meteor.,* **10,** 780–784.

Bowen, E. G., 1952: A new method of stimulating convective clouds to produce rain and hail. *Quart. J. Roy. Meteor. Soc.,* **78,** 37–45.

Cooper, W. A., and R. P. Lawson, 1984: Physical interpretation of results from the HIPLEX-1 experiment. *J. Climate Appl. Meteor.,* **23,** 523–540.

——, R. T. Bruintjes, and G. K. Mather, 1997: Some calculations pertaining to hygroscopic seeding with flares. *J. Appl. Meteor.,* **36,** 1449–1469.

Czys, R. R., and R. T. Bruintjes, 1994: A review of hygroscopic seeding experiments to enhance rainfall. *J. Wea. Mod.,* **26,** 41–52.

Fitzgerald, J. W., 1974: Effect of aerosol composition on cloud droplet size distribution: A numerical study. *J. Atmos. Sci.,* **31,** 1358–1367.

Krauss, T. W., R. T. Bruintjes, J. Verlinde, and A. Kahn, 1987: Microphysical and radar observations of seeded and unseeded continental cumulus clouds. *J. Climate Appl. Meteor.,* **26,** 585–606.

Mather, G. K., and D. E. Terblanche, 1992: Cloud physics experiments with artificially produced hygroscopic nuclei. *Proc. 11th Int. Conf. on Cloud Physics,* Montreal, PQ, Canada, International Commission on Cloud and Precipitation, IAMAP, 147–150.

——, ——, F. E. Steffens, and L. Fletcher, 1997: Results of the South African cloud-seeding experiments using hygroscopic flares. *J. Appl. Meteor.,* **36,** 1433–1447.

Mordy, W., 1959: Computation of the growth by condensation of a population of cloud droplets. *Tellus,* **11,** 16–44.

Pruppacher, H. R., and J. D. Klett, 1997: *Microphysics of Clouds and Precipitation.* D. Reidel, 714 pp.

Reisin, T., S. Tzivion, and Z. Levin, 1996a: Seeding convective clouds with ice nuclei or hygroscopic particles: A numerical study using a model with detailed microphysics. *J. Appl. Meteor.,* **35,** 1416–1434.

——, Z. Levin, and S. Tzivion, 1996b: Rain production in convective clouds as simulated in an axisymmetric model with detailed microphysics. Part I: Description of the model. *J. Atmos. Sci.,* **53,** 497–519.

Takeda, T., and N. Kuba, 1982: Numerical study of the effect of CCN on the size distribution of cloud droplets. Part I: Cloud droplets in the stage of condensation growth. *J. Meteor. Soc. Japan,* **60,** 978–993.

Twomey, S., and T. A. Wojciechowski, 1969: Observations of the geographical variation of cloud nuclei. *J. Atmos. Sci.,* **26,** 684–688.

Tzivion, S., G. Feingold, and Z. Levin, 1987: An efficient numerical solution to the stochastic collection equation. *J. Atmos. Sci.,* **44,** 3139–3149.

——, ——, and ——, 1989: The evolution of raindrop spectra. Part II: Collisional collection/breakup and evaporation in a rainshaft. *J. Atmos. Sci.,* **46,** 3312–3327.

——, T. Reisin, and Z. Levin, 1994: Numerical simulation of hygroscopic seeding in a convective cloud. *J. Appl. Meteor.,* **33,** 252–266.

Yin, Y., Z. Levin, T. G. Reisin, and S. Tzivion, 2000: The effects of giant cloud condensation nuclei on the development of precipitation in convective clouds—A numerical study. *Atmos. Res.,* **53,** 91–116.

Unauthenticated | Downloaded 07/13/24 07:39 PM UTC